DTC, DPC and Nonlinear Vector Control Strategies Applied to the DFIG Operated at Variable Speed

Jihène Ben Alaya[1,3] , Adel Khedher[2,4] , Mohamed Faouzi Mimouni[1,5]

Réseaux et Machines Electriques (RME) [1],
Renewable Energy and Electric Vehicles (RELEV) [2]
Training Professional Center of M'Saken, 4070 M'Saken -Tunisia[3]
National Engineering School of Sousse, 4054 Sousse-Tunisia[4]
National Engineering School of Monastir, 5000 Monastir-Tunisia[5]

bnajihene@yahoo.fr, adel_kheder@yahoo.fr, mfaouzi.mimouni@enim.rnu.tn

Abstract: - In this paper we present the modeling and control designs for a variable-speed constant-frequency wind energy conversion system using double fed induction generator (DFIG). The aim of this paper is to design and compare two distinct control strategies to control the rotor side power converter and two control strategies to control the grid side power converter. For the rotor side converter (RSC), a nonlinear vector control strategy using the second *Lyapunov* approach is firstly developed. Secondly, a direct torque control strategy, constructed around two hysteresis controllers that allow flux and torque regulation, is presented. For the grid side converter (GSC), the network voltage vector oriented control based on PI controllers and a direct power control strategy constructed around two hysteresis controllers that allow grid injected power regulation, are presented, respectively. Simulation results have shown good performances of the wind energy converter system operate under typical wind variations and every propose control strategies.

Key-Words: - Double fed induction generator - Direct torque control - Nonlinear vector control -*Lyapunov* approach - Network voltage oriented control - Direct power control.

1 Introduction

To produce electrical energy using a wind energy conversion system (WECS), various control strategies have been developed in the literature [1-12]. The most widely used control techniques are the vector control (VC) [1-4] and the direct control techniques [5-8]. All this techniques have the goal to bring down the cost of electrical energy produced by the WECS and to converge the system for operating at unity power factor.

For the rotor side converter (RSC), the VC strategy which guarantees high dynamics and static performance via an internal current control loops, has attracted much attention in the past few decades. However, the performance of the VC largely depends on the design of the current controllers and the tuning of their parameters [3,4].

Direct Control eliminates the need for current regulators and specific modulations. Direct torque control (DTC) provides direct control of machine's torque and flux. This approach achieves better steady state and transient torque control conditions, but it is penalized by the electromagnetic torque noises and the high switching frequency [11,17].

The grid side converter (GSC) can also be controlled by VC technique [1,9,10,11]. This method guarantees a high static performance but it is affected by the stability requirements of the feedback loops.

In the last few years, the use of direct control techniques like the DPC witch select the converter switching patterns from an optimal switching table based on the instantaneous errors of the active and reactive powers, and the angular position of the converter terminal voltage vector, for high power systems like WECS, is spreading due to the advantages, such as a fast dynamics and simplicity, when compared with other methods [13,14].

The aim of this paper is to present, discuss and compare various control strategies for DFIG driven by wind turbine under typical wind variations. The DFIG will be connected to a rural grid directly by the stator and through a back to back converter by the rotor. This structure has the advantage of using power converter rated for approximately 30% of the total exchanged power, which makes this solution more suitable for variable speed wind turbines [9,12].

For the RSC, a non linear vector control (NLVC) and a direct torque control (DTC) will be developed. Without any internal current control loops, the proposed NLVC technique allow to overcome the problems of the classical field oriented control. It is based on the second approach of *Lyapunov* theory which rests on the definition of positive definite candidate function V whose convergence towards zero generate the convergence of the state of the system towards its equilibrium. In this study, the definition of the candidate function is based on the minimization of the energy criterion. The DTC strategy controls directly the electromagnetic torque and flux by selecting voltage vectors from a look-up-table. In DTC, the flux is conventionally obtained from the rotor voltage model, using the measured rotor voltages and currents [5,6]. This method, utilizing open-loop pure integration, suffers from increased noise on voltage and current and quantization errors in the digital system, in addition to the offset gain and conversions factors in the low speed range, even with the correct knowledge of the rotor resistance. In this paper, the proposed DTC approach uses the measured stator and rotor currents to estimate flux and torque. For both proposed control strategies, we will maximize the energy captured from the wind turbine and injected to the grid.

For the GSC, the network voltage vector oriented control (NVVOC) based on PI controllers will be firstly presented. Secondly, the DPC technique will be developed. In [13,14], the reference powers line are calculated using information about the DC-link voltage. In this study, the proposed DPC algorithm not requires DC-link voltage controller and the reference powers are definite proportional to the maximum mechanical power extracted from the wind turbine.

This paper is organized as follows in the second section; we present the model of the DFIG and of the wind turbine. Third section presents the control strategies of the RSC. Firstly, we propose a NLVC based on the second approach of *Lyapunov*. Then, the DTC principle is developed. Fourth section, studies the control of electrical system in the GSC. Firstly, we propose a NVVOC. Then, the DPC principle is developed. Simulation results are presented and discussed in the fifth section and we finish by a conclusion.

2 DFIG model

In complex notation, the DFIG mechanical and electrical equations are derived from *Park* model expressed in a reference frame d-q rotating at synchronous speed ω_s as follows [9].

$$\begin{cases} \dfrac{d\bar{i}_s}{dt} = -a_{ss}\bar{i}_s + a_{sr}\bar{i}_r + b_{ss}\bar{v}_s - b_{sr}\bar{v}_r \\ \dfrac{d\bar{i}_r}{dt} = a_{rs}\bar{i}_s - a_{rr}\bar{i}_r - b_{sr}\bar{v}_s + b_{rr}\bar{v}_r \\ (J_m + \dfrac{J_t}{m^2})\dfrac{d\omega}{dt} + f\omega = \dfrac{T_t}{G} - T_{em} \end{cases} \quad (1)$$

All electrical and mechanical variables and notations are defined in appendix1.

With:

$$a_{ss} = \frac{1}{\sigma\tau_s} + j(\frac{\omega_s}{\sigma} - \frac{\omega_g M^2}{\sigma L_s L_r})$$

$$a_{sr} = \frac{M}{\sigma L_s \tau_r} + j\frac{M}{\sigma L_s}(\omega_g - \omega_s)$$

$$a_{rs} = \frac{M}{\sigma L_r \tau_s} + j\frac{M}{\sigma L_r}(\omega_s - \omega_g)$$

$$a_{rr} = \frac{1}{\sigma\tau_r} + j(\frac{\omega_g}{\sigma} - \frac{\omega_s M^2}{\sigma L_s L_r})$$

$$b_{ss} = \frac{1}{\sigma L_s};\ b_{sr} = \frac{M}{\sigma L_s L_r};\ b_{rr} = \frac{1}{\sigma L_r}$$

Using stator and rotor space vector currents, the electromagnetic torque generated by the DFIG is given by:

$$T_{em} = \frac{3}{2} p M \Im m(\bar{i}_s \bar{i}_r^*) \quad (2)$$

The developed wind turbine torque is given by [7]:

$$T_t = \frac{\rho\pi R_b^2 V_v^3}{2\Omega_t} C_p \quad (3)$$

In this study, for each wind speed the rotational speed is varied to track the maximum power curve as shown in fig.1. The maximum mechanical power extracted from the wind turbine is given by:

$$P_{t\max} = \frac{1}{2}\rho\pi R_b^2 V_v^3 C_{p\max} \quad (4)$$

The optimum power produced by the turbine vs. electrical speed can be described by the following polynomial equation:

$$\begin{cases} P_t = 0.081\omega^3 + 5.1\omega^2 & \text{if} \quad V_v < 25\text{m/s} \\ \quad -1.310^2\omega + 3.410^4 & \\ P_t = 3.4MW & \text{if} \quad V_v \geq 25\text{m/s} \end{cases} \quad (5)$$

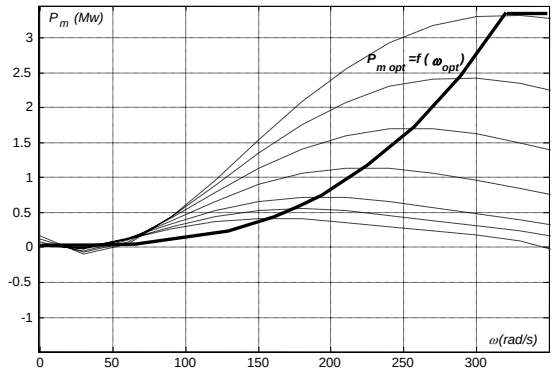

Fig.1 Mechanical turbine power variations for different wind speed levels

The active and reactive powers exchanged between the stator and the grid are given by:

$$\begin{cases} P_s = \frac{3}{2}\Re e(\overline{v_s}\,\overline{i_s}^{*}) \\ Q_s = \frac{3}{2}\Im m(\overline{v_s}\,\overline{i_s}^{*}) \end{cases} \quad (6)$$

In this paper, the reference powers are specified in order to extract the maximum power from wind energy for a given wind speed and to operate at unity power factor.

Stator and rotor currents are expressed as follows:

$$\begin{cases} \overline{i_s} = b_{ss}\overline{\varphi}_s - b_{sr}\overline{\varphi}_r \\ \overline{i_r} = b_{rr}\overline{\varphi}_r - b_{sr}\overline{\varphi}_s \end{cases} \quad (7)$$

The DFIM equations derived from *Park* model given by (1), can be expressed using rotor and stator flux vectors as follows:

$$\begin{cases} \frac{d\overline{\varphi}_s}{dt} = -f_{ss}\overline{\varphi}_s + f_{sr}\overline{\varphi}_r + \overline{v}_s \\ \frac{d\overline{\varphi}_r}{dt} = f_{rs}\overline{\varphi}_s - f_{rr}\overline{\varphi}_r + \overline{v}_r \\ T_{em} = \frac{3}{2}p\frac{M}{\sigma L_s L_r}\Im m(\overline{\varphi_s}\,\overline{\varphi_r}^{*}) \end{cases} \quad (8)$$

With:

$$f_{ss} = \frac{1}{\sigma\tau_s} + j\omega_s \;;\; f_{sr} = \frac{M}{\sigma\tau_s L_r} \;;$$

$$f_{rs} = \frac{M}{\sigma\tau_r L_s} \;;\; f_{rr} = \frac{1}{\sigma\tau_r} + j\omega_g$$

3 RSC control

The general structure of the WECS proposed in the work is given by fig.2. In this part, we present two control strategies. The first is a nonlinear vector control based on the *Lyapunov* stability theory. The second is the direct torque control strategy.

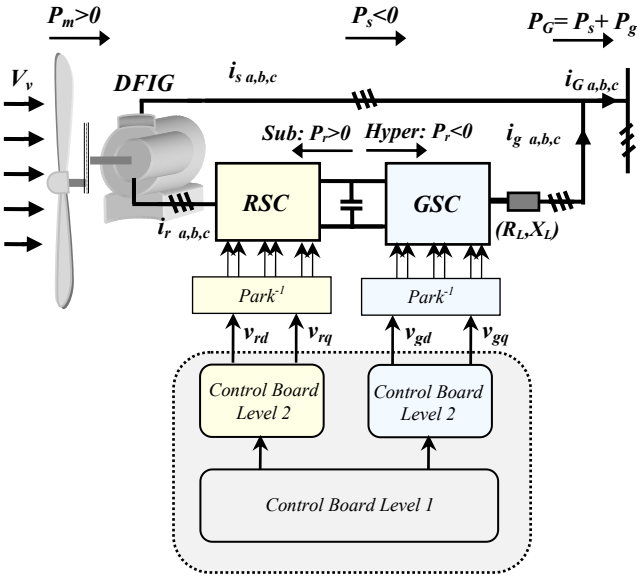

Fig.2 Control structure of the proposed WECS

3.1 NLVC based on the Lyapunov approach

For large power generator, we can neglect the effect of stator resistance face the stator voltage and magneto-motive force. So, in a *Park* reference frame linked to the stator flux, the stator voltage vector is consequently in quadratic advance with the stator flux vector. This implies that:

$$\begin{cases} \varphi_{sd} = \varphi_s \,, \varphi_{sq} = 0 \\ v_{sq} = v_s \end{cases} \quad (9)$$

With this consideration, for each value of stator flux we can control the stator active and reactive powers by the quadrature and the direct rotor currents respectively [8,9].

The stability study of the system is based on the definition of a candidate function V which convergence towards zero constitutes the principle stability condition of the system. In this study, one considers a function of *Lyapunov*, definite positive, which minimizes the energy criterion, as follows:

$$\begin{aligned} V &= \frac{1}{2}(P_s - P_{sref})^2 + \frac{1}{2}(Q_s - Q_{sref})^2 \\ &= \frac{1}{2}(\Delta P_s)^2 + \frac{1}{2}(\Delta Q_s)^2 \end{aligned} \quad (10)$$

According to *Lyapunov* theory the system is stable if the derivative of V is definite negative [15].

$$\dot{V} = (P_s - P_{sref})(\dot{P}_s - \dot{P}_{sref}) + (Q_s - Q_{sref})(\dot{Q}_s - \dot{Q}_{sref}) \quad (11)$$

Where:

$\dot{P}_s$ et $\dot{Q}_s$ represent respectively, the derivative of the active and reactive stator powers.

Let be considering the following function:

$$\begin{cases} f_1 = \Re e(-f_{ss}\,\overline{\varphi_s} + f_{sr}\,\overline{\varphi_r}) \\ f_2 = \Im m(-f_{ss}\,\overline{\varphi_s} + f_{sr}\,\overline{\varphi_r}) \\ f_3 = \Re e(f_{sr}\,\overline{\varphi_s} - f_{rr}\,\overline{\varphi_r}) \\ f_4 = \Im m(f_{rs}\,\overline{\varphi_s} - f_{rr}\,\overline{\varphi_r}) \end{cases} \quad (12)$$

By applying the hypothesis of orientation of flux and of voltage to the systems (8) the relation (11) becomes:

$$\dot{V} = \Delta P_s\left[\frac{-3M}{2\sigma L_s L_r} v_{sq}\,(f_4 + v_{rq}) - \dot{P}_{sref}\right] + \Delta Q_s\left[\left(\frac{3v_{sq}}{2\sigma L_s} f_1 - \frac{3M}{2\sigma L_s L_r} v_{sq}(f_3 + v_{rd})\right) - \dot{Q}_{sref}\right] \quad (13)$$

Knowing that to satisfy the energy criterion the derivative of *Lyapunov* function must be definite negative, one defines then two numbers K_p and K_q strictly positive, such as:

$$\dot{V} = -K_p\,(P_s - P_{sref})^2 - K_q\,(Q_s - Q_{sref})^2 \quad (14)$$

K_p and K_q should be chosen such that they satisfy the following conditions:

$$\begin{cases} K_p \geq \dfrac{1}{\Delta P_s}\left[\dfrac{3M}{2\sigma L_s L_r} v_{sq}\,(f_4 + v_{rq}) + \dot{P}_{sref}\right] \\ K_q \geq \dfrac{1}{\Delta Q_s}\left[\dfrac{-3v_{sq}}{2\sigma L_s} f_1 + \dfrac{3M}{2\sigma L_s L_r} v_{sq}(f_3 + v_{rd}) + \dot{Q}_{sref}\right] \end{cases} \quad (15)$$

The control voltages of RSC are consequently expressed as follows:

$$\begin{cases} v_{rd} = \dfrac{2\sigma L_s L_r}{3M\,v_{sq}}\left(\dfrac{3}{2\sigma L_s} f_1 v_{sq} - \dfrac{3M}{2\sigma L_s L_r} f_3 v_{sq} - \dot{Q}_{sref} + K_q\,\Delta Q_s\right) \\ v_{rq} = \dfrac{2\sigma L_s L_r}{3M\,v_{sq}}\left(-\dfrac{3M}{2\sigma L_s L_r} f_4 v_{sq} - \dot{P}_{sref} + K_p\,\Delta P_s\right) \end{cases} \quad (16)$$

The RSC control broad level 2 is illustrated by Fig.3.

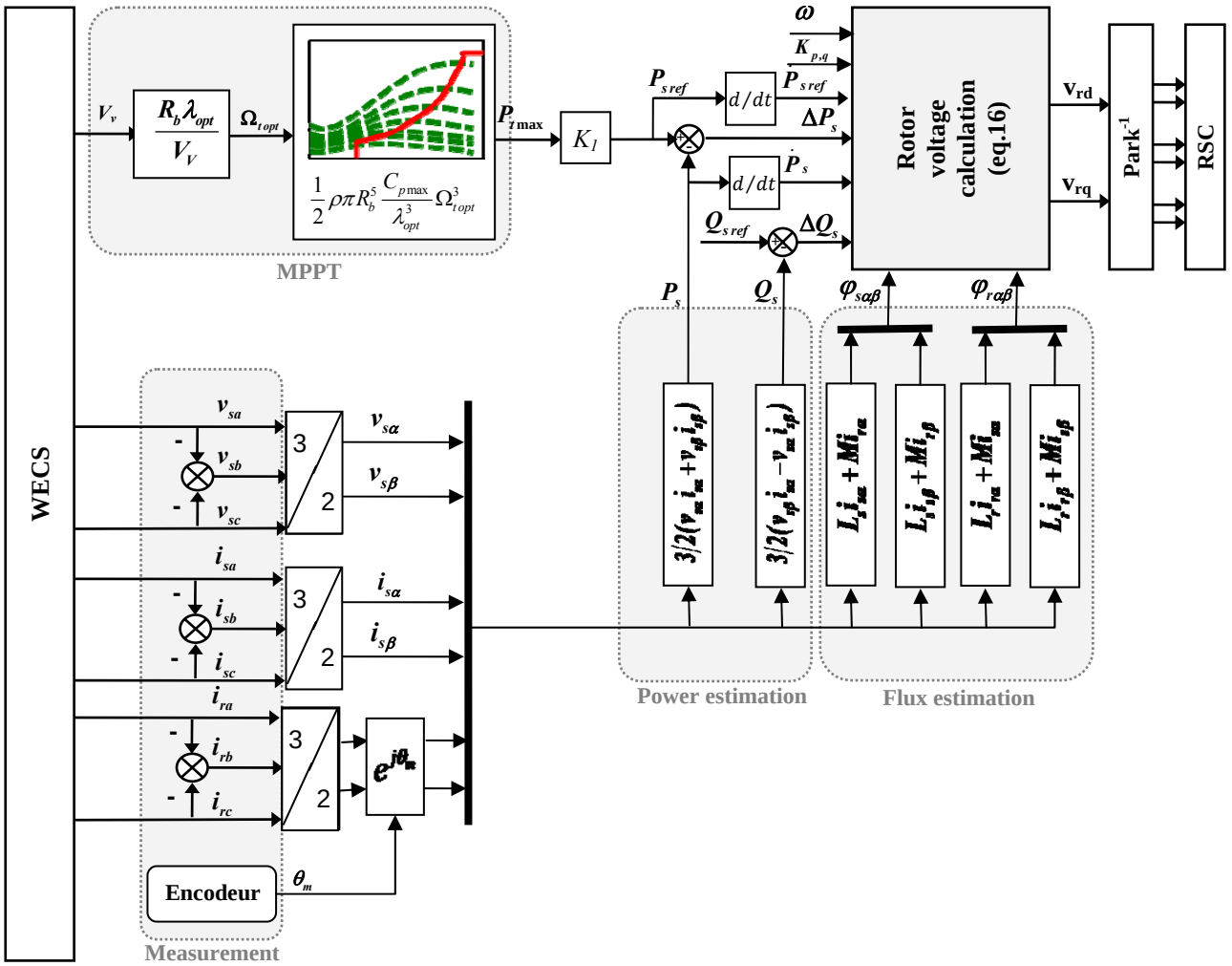

Fig.3 RSC control broad level 2: NLVC

3.2 Direct torque control

Direct torque control is derived by the fact that, on the basis of the errors between the reference and the estimated values of electromagnetic torque and flux, it is possible to directly control the inverter states in order to reduce the torque and flux errors within the prefixed band limits. The used DTC in our case is based on the same principle as for squirrel cage induction machine [11,16,17,18]. The flux controller is based on a two level hysteresis comparator with H_F hysteresis band illustrated by Fig.4.a, while the electromagnetic torque controller uses a three level hysteresis comparator with H_T hysteresis band illustrated by Fig.4.b.

In order to reduce torque and flux ripples, the hysteresis bands width of both controllers (H_T and H_F) should be set to small values. In practice, those values are limited by the minimum switching sample period of the hardware used for the implementation [11,17].

The rotor flux space evolution is divided into six sector (N_{sk}).When rotor flux is in a sector (k), the control of flux and torque can be ensured by selecting one of the eight following voltage vector:

$$\begin{cases} V_k = \sqrt{\frac{2}{3}} v_{dc} e^{j\frac{\pi}{3}(k-1)} & k \in [1,6] \\ V_0 = V_7 = 0 \end{cases} \quad (17)$$

So, the voltage vector selection is carried out according following table 1.

In this paper, rotor flux estimation uses measured stator and rotor currents. So, the rotor flux linkage vector is estimated in the stator reference frame using the following equation:

$$\bar{\varphi}_{re}^{s} = L_r \bar{i}_r^{r} e^{j\theta_m} + M \bar{i}_s^{s} \quad (18)$$

Table 1. Rotor voltage vector selection according to torque and flux errors

Flux	Torque	e_T = 1	e_T = 0	e_T = -1
e_φ	1	V_{k-1}	V_0 , V_7	V_{k+1}
	-1	V_{k-2}	V_0 , V_7	V_{k+2}

The location of the rotor flux vector represents the actual sector and it is computed as follows:

$$\alpha_r = atg\left(\frac{\varphi_{r\beta e}}{\varphi_{r\alpha e}}\right) \quad (19)$$

The estimate electromagnetic torque T_{eme} is directly calculated from the measured currents and the machine parameters as follows:

$$T_{eme} = \frac{3}{2} pM \Im m(\bar{i}_s \bar{i}_r^{*}) \quad (20)$$

The structure of the direct torque control is illustrated by Fig.5.

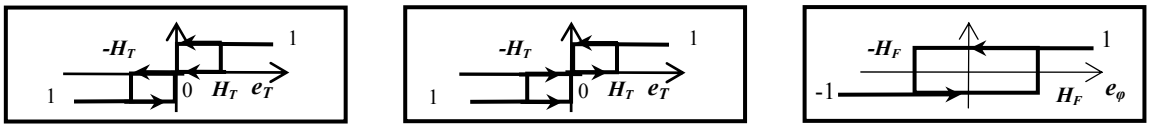

(a1) (a2) (b)

Fig.4 (a) Electromagnetic torque hysteresis comparator:
(a_1) Subsynchronism, (a_2) Hypersynchronism, (b) Rotor flux hysteresis comparator.

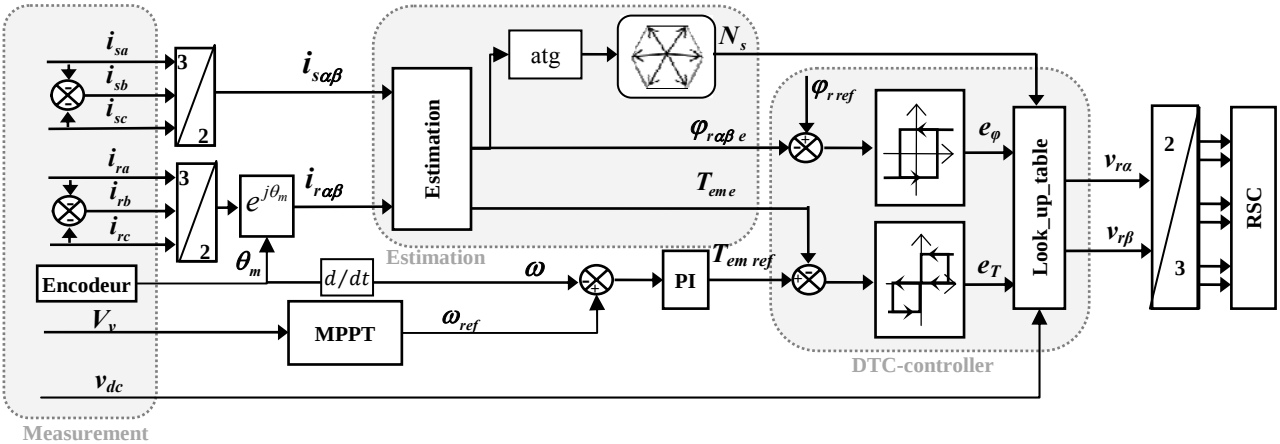

Fig.5 RSC control broad level 2: DTC

4 GSC control

The GSC is equipped by a two-stage controller operating in a grid AC voltage reference frame. It controls the power flow exchange with the grid via the rotor. The GSC current output is determinate by *Kirchhoff laws* applied at the connection between the grid and the wind generation system as follows:

$$\bar{v}_g - \bar{v}_G = (R_L + jX_L)\,\bar{i}_g + L_L \frac{d\bar{i}_g}{dt} \tag{21}$$

With:

$$\begin{cases} \bar{v}_G = \bar{v}_s \\ \bar{i}_G = \bar{i}_s + \bar{i}_g \end{cases} \tag{22}$$

The grid powers at the connection between the grid and the wind generation system are given by:

$$\begin{cases} P_G = P_s + P_g \\ Q_G = Q_s + Q_g \end{cases} \tag{23}$$

The power in the dc bus is expressed as:

$$P_{dc} = \frac{dW_{dc}}{dt} = Cv_{dc}\frac{dv_{dc}}{dt} \tag{24}$$

In terms of different losses and powers, P_{dc} can be also written as follows:

$$P_{dc} = P_m - P_{loss,s} - P_{loss,r} - P_s - P_g \tag{25}$$

With:

$$\begin{aligned} P_m &= T_{em}\frac{\omega}{p} \\ P_{loss,s} &= \frac{3}{2}R_s(i_{s\alpha}^2 + i_{s\beta}^2)\ , \\ P_{loss,r} &= \frac{3}{2}R_r(i_{r\alpha}^2 + i_{r\beta}^2) \\ P_s &= \frac{3}{2}\Re e(\bar{v}_s^{\,s}\,\bar{i}_s^{\,s*}) \\ P_g &= \frac{3}{2}\Re e(\bar{v}_G^{\,s}\,\bar{i}_g^{\,s*}) \end{aligned} \tag{26}$$

For the GSC, we present two control strategies. The firstly is the NVVOC based on four PI controllers and the voltage compensation method, the secondly is the DPC strategy constructed around two hysteresis controllers that allow grid injected power regulation.

4.1 NVVOC

The NVVOC strategy principle consists in orienting the d-axis *Park* frame (rotating at synchronous speed) according to the network voltage. This implies that:

$$\begin{cases} v_{Gd} = |\bar{v}_G| \\ v_{Gq} = 0 \end{cases} \tag{27}$$

In these conditions, one can write:

$$\begin{cases} P_g = \frac{3}{2}v_{Gd}i_{gd} \\ Q_g = -\frac{3}{2}v_{Gd}i_{gq} \end{cases} \tag{28}$$

Thus, the dynamics of the active and reactive powers becomes directly linked to the control of network currents components [9,10]. Fig.6 illustrates the proposed NVVOC strategy. For this algorithm, the dc-bus reference voltage is constant and equal to the nominal AC voltage.

4.2 DPC

The basic idea of the DPC approach is the direct control of active and reactive power injected to the grid via the GSC without any internal control loop or PWM modulator.

Converter switching states are selected from an optimal switching table based on the instantaneous errors of active and reactive powers and of the angular position of the vector voltage as illustrated by Fig.7. The selection of the voltage vector is carried out with the same principle of the DTC [18,19].

To calculate the reference GSC powers and to operate at unity stator power factor, we have neglected the stator and rotor windings' copper losses and the loss power in the dc-bus. So, they are chosen as follows:

$$\begin{cases} P_{g\,ref} = K_2 P_{t\max} \\ Q_{g\,ref} = 0 \end{cases} \tag{29}$$

Knowing that the total active power generated by a DFIG system is the sum of the active power outputs from the DFIG stator and the GSC as expressed in (23), with the proposed hypothesis, we can express the electromagnetic power as follows :

$$P_m = P_G = P_s + P_r \tag{30}$$

With:

$$P_r = g\,P_s$$

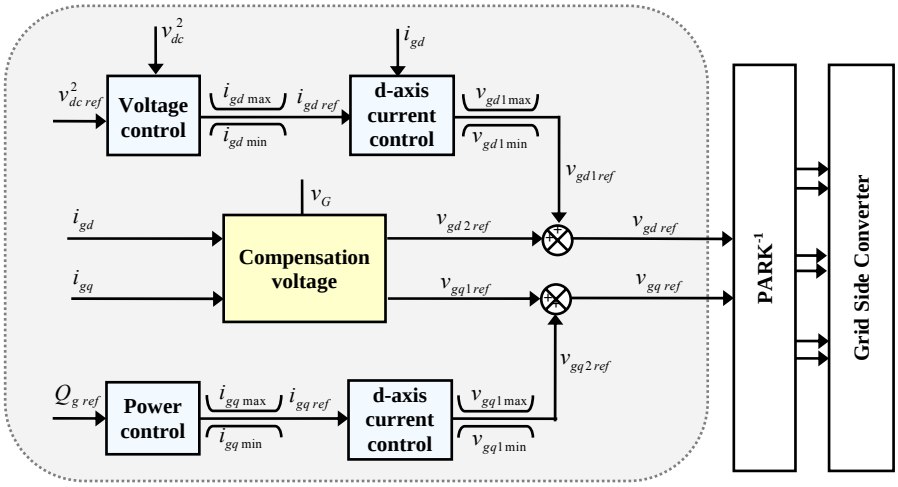

Fig.6 GSC control broad level 2: NVVOC

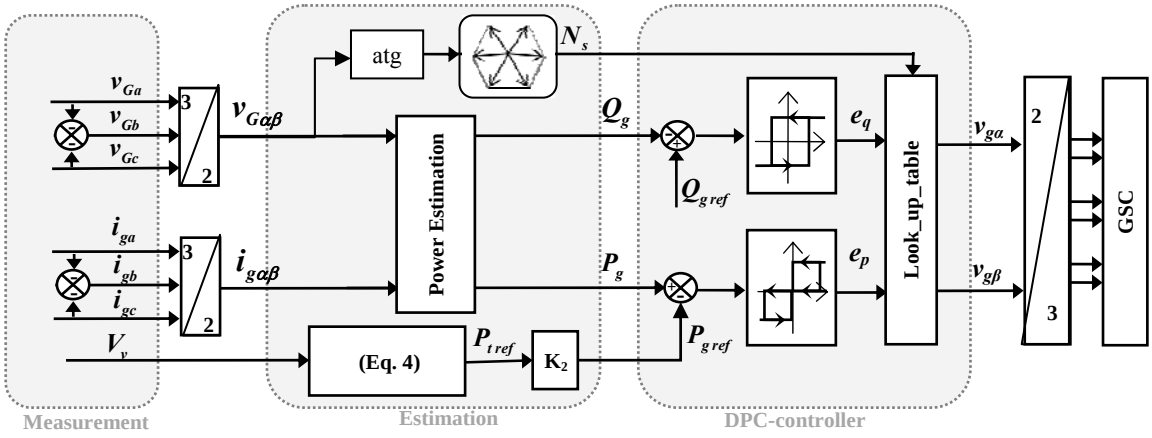

Fig.7 GSC control broad level 2: DPC

5 Simulation results

Simulations results are made by using the real parameters of a wind turbine AE43 and a DFIG rated at 660KW and 690V.

The operation of the WECS is simulated under the following combinations of different control strategies. Simulations results are summarized in the table 2.

Table 2: Summarization table of simulation results illustrations

	RSC	GSC	Fig.	Location
Case 1	NLVC	NVVOC	10-11	Left
Case 2	DTC	NVVOC	10-11	Right
Case 3	NLVC	DPC	12-13	Left
Case 4	DTC	DPC	12-13	Right

In order to made a comparison between the proposed control strategies, all the simulations are carried out in the same operation conditions, i.e.:

- The rotor flux reference is chosen equal to 3.1Wb (rated value).
- The dc-voltage reference is equal to 1700V.
- The chosen wind speed profile is illustrated by Fig.8.

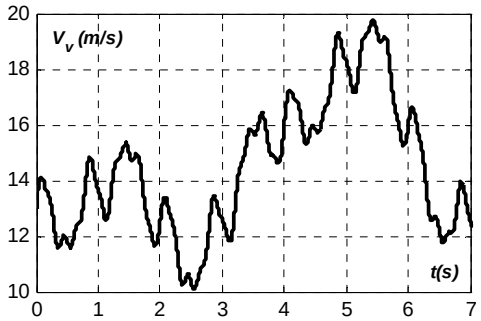

Fig.8 Wind speed profile

- The WECS is controlled at unity power and the slip range from -30% to 30%, as illustrated in Fig.9.

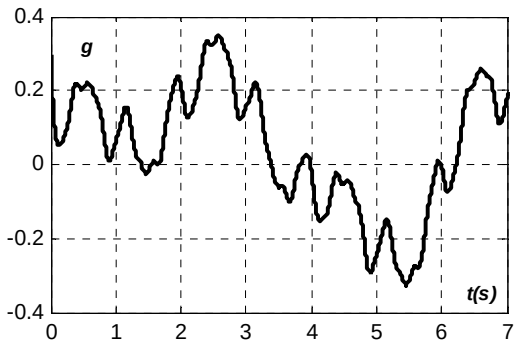

Fig.9 Slip variation of the grid-connected DFIG

As it can be seen in Fig.10, 12(a,b), the combinations of proposed control strategies are able to follow the wind speed changes rapidly despite the important fluctuations of the wind speed and the big inertia of the machine.

The use of the DTC influence the location of system operation mode. Indeed, as shown in electromagnetic torque variations illustrate by Fig.10, 12(c,d), we observe that for a peak of wind speed, the WECS switches between the generating mode ($T_{em}<0$) and the motoring mode ($T_{em}>0$) witch introduce a sudden jump in the stator power factor (SPF) illustrated by Fig.11,13(f). Something that does not occur for NLVC strategy combined with NVVOC or DPC strategies due to the convergence towards zero of the *Lyapunov* function. Indeed, the stator power factor, illustrated by Fig.11,13(e), converges to -1 confirming the null-VAR generating mode.

Moreover, this wind variations have an effect on the transient's active power variations, illustrated by Fig.11,13(d) and the current injected to the grid, illustrated by Fig.11,13(h).

The stator flux is shown in Fig. 10,12(e,f). The proposed approaches allows a quick stator flux response justified by the directly connection between the stator and the grid. However, one can register in the DTC cases a stator flux peak equal to the double of the rated value.

Fig.10,12(h) show that the hysteresis controller in the DTC strategy allow a well and quickly rotor flux regulation and we notice that the GSC control strategies haven't consequence on this regulation. However, with NLVC strategy, the rotor flux is affected by wind variations and we notice that the GSC control has influence on the rotor flux variations which is limited by the DPC strategy. Indeed, as we can show in Fig.10,12(g), an increase , respectively, a decrease of the wind; introduce an increase, respectively, a decrease, of the rotor flux especially in the hyper synchronous mode.

It is important to highlight that for all the proposed algorithms the currents in the three phase's network, illustrate by Fig.11,13(g,h), constitute a balanced system of the rural network frequency.

6 Conclusion

This work treated some control strategies applied of the wind energy conversion system (WECS) based on the double fed induction generator (DFIG). We have designed and compared two control strategies for the rotor side converter (RSC): a direct torque control (DTC) and a nonlinear vector control (NLVC) using the second approach of *Lyapunov* and two control strategies for the grid side converter (GSC): a network vector voltage oriented control (NVVOC) and a direct power control (DPC). The bi-directional power converters allow the power energy to transit between the local grid and the WECS.

For every proposed case, the system operates at maximum power generation mode. Simulation results of four combine control strategies NLVC-NVVOC, DTC-NVVOC, NLVC-DPC and DTC-DPC, illustrated in table 2, have proven that the proposed algorithms are able to offer convergence of the dynamic response of the system to the reference values despite wind variations. The case number 3, NLVC-DPC strategy is a good candidate for controlling the WECS based on a DFIG interconnected to the grid.

Appendix

Induction generator data

Rated power: 660 kW, Rated stator voltage: 400/690V, 50Hz, R_r=0.0238Ω, R_s=0.0146Ω, L_s=0.0306 H, L_r=0.0303H, M=0.0299H, J_m=28kg.m^2, p=2,

Wind turbine data

Number of blades=3, Rotor diameter: $2R_b$=43m, Gearbox coefficient: G= 55.747, Cut-in wind speed: $V_{v,min}$=3m/s, Cutoff wind speed: $V_{v,max}$=25m/s, Optimal tip speed ratio: λ_{opt}=4, J_t=238kg.m^2, f=26,

Grid parameters

Network rated voltage: v_G =975V, 50Hz, R_L=3Ω, L_L=0.051H.

Power coefficient expression

$$C_p = \sum_{i=0}^{5} a_i \lambda^i$$

With:

a_5=-0.000373, a_4=0.009309, a_3=-0.081857, a_2=0.2774,a_1=-0.19084, a_0=0.021945.

Nomenclature

i_s, i_r Stator, rotor current vector (A).
v_s, v_r Stator, rotor voltage vector (V).
T_{em} Electromagnetic Torque (Nm).

J, f Inertia and viscous friction.
φ_s, φ_r Stator, rotor flux linkage vector (Wb).
P_s, Q_s Stator active, reactive power.
P_r, Q_r Rotor active, reactive power.
$\omega_s, \omega, \omega_g$ Synchronous, rotor and slip speeds (rad/s).
R_s, R_r Stator, rotor resistance (Ω).
M Mutual inductance.
L_s, L_r Stator, rotor total cyclic inductance
p Machine pole pairs.
V_v Wind speed (m/s).
T_t Wind turbine Torque (Nm).
C_p Power coefficient
λ Tip speed ratio
v_g, v_G Output grid side converter, grid voltage vector (V).
i_g, i_G Output grid side converter, grid current vector (V).
R_L, X_L Line resistance, inductance.
e_φ Rotor flux error
e_T Electromagnetic torque error
e_p Active power error
e_q Reactive power error
σ Leakage factor, $\sigma = 1 - \frac{M^2}{L_s L_r}$

Subscripts
a,b,c Quantities in *a,b* and *c*-axis
α,β Quantities in *α*-axis and *β*-axis
d,q Quantities in *d*-axis and *q*-axis
ref Reference value.
e Estimated value.

Superscripts
s Stationary reference frame
r Rotor reference frame

References

[1] M. Salles, J.R. Cardoso, A.P. Grilo, C. Rahmann, K. Hameyer. Control strategies of doubly fed induction generators to support grid voltage. *IEEE International Conference on Electric Machines and Drives (IEMDC '09).* 3-6 May 2009. pp. 1551-1556.

[2] A. Chikhil. A Comparative Study of Field-Oriented control and direct torque control of Induction Motors using an adaptive flux observer. *Journal of Electrical Engineering.* Vol.10, Issue 3.2010. pp.91-97.

[3] A. Tapia, G. Tapia, J.X. Ostolaza, J.R. Saenz. Modeling and control of a wind turbine driven doubly fed induction generator. *IEEE Trans. Energy Conversion.* Vol.18, Issue 2. June 2003. pp. 194-204.

[4] J. Hu, Y. He, L. Xu, B.W. Williams. Improved Control of DFIG Systems During Network Unbalance Using PI–R Current Regulators. *IEEE Trans Industrial Electronics*. Vol. 56, Issue 2. February 2009. pp.439-451.

[5] X. Zuoxia, Y. Xingjia, S. Hongxia, T.Q. Zheng. DTC in Doubly-fed VSCF wind turbine control system. IEEE Industrial Technology, ICIT'06. December 2006. pp.2715-2718.

[6] F. Bonnet, P.E. Vidal, M. Pietrzak-David. Dual Direct Torque Control of Doubly Fed Induction Machine. *IEEE Trans. Industrial Electronics.* Vol.54, No.5. October 2007. pp. 2482-2490.

[7] K.C. Wong, S.L. Ho, K.W.E. Cheng. Direct control algorithm for doubly fed induction generators in weak grids. *Electric Power Applications, IET.* Vol.3, Issue 4. July 2009. pp. 371-380.

[8] C. Belfedal S. Moreau. A.A. Naassani M.A Denai. T. Allaoui. Comparison of PI and Hysteresis Control of the Active and Reactive Power of Doubly Fed Induction Generator Fed by Three-Level Inverter. *Journal of Electrical Engineering.* Vol.5, Issue 2. 2005. pp. 56-63.

[9] J. Ben Alaya, A. Khedher, M.F. Mimouni. Variable Speed Vector Control Strategy of the Double Fed Induction Generator Integrated in Electrical Grid. *International Conference on Ecologic Vehicles and Renewable Energy (EVER'08)*, Monaco, France. March 2008.

[10] L. Shuhui, T.A. Haskew. Analysis of Decoupled d-q Vector Control in DFIG Back-to-Back PWM Converter. *IEEE CNF Power Engineering.* June 2007. pp.1-7.

[11] J. Ben Alaya, A. Khedher, M.F. Mimouni. Direct Torque Control and Network Vector Voltage Oriented Control of DFIG Integrated in Electrical Grid. *International Conference on Electrical Systems and Automatic Control (JTEA'09),* Hammamet, Tunisia. March 2009.

[12] A. K. Mishra, L. Ramesh, S.P. Chowdhury, S.Chowdhury. Review of Wind Turbine System and its Impact for Grid Stability. *Journal of Electrical Engineering.* Vol.11, Issue 1. 2011. pp. 153–165.

[13] L. A. Serpa, J. W. Kolar. Virtual-Flux Direct Power Control for Mains Connected Three-Level NPC Inverter Systems. *Proceedings of the 4th Power Conversion Conference (PCC'07)*, Nagoya, Japan, April 2007.

[14] S.A. Larrinaga, M.A.R. Vidal, E. Oyarbide, J.R.T. Apraiz. Predictive Control Strategy for DC/AC Converters Based on Direct Power Control. *IEEE Trans. Industrial Electronics*. Vol. 54, No. 3. June 2007. pp. 1261-1271.

[15] V.G. Rau, G. Durga Prasad. Dynamic stability assessment of wind turbine generators using the Lyapunov function approach. *Electric Power Systems Research.* Vol.27, Issue 1. May 1993. pp. 61-72.

[16] I. Takahashi, Y. Ohmori. High-Performance Direct Torque Control of an Induction Motor. *IEEE Trans. Industry Applications*. Vol.25, No.2. March/April 1989.

[17] A. Khedher, M.F. Mimouni. Sensorless-adaptive DTC of double star induction motor. *Journal of Energy Conversion and Management.* Issue 51. December 2010. pp. 2878–2892.

[18] X. Zuoxia, Y. Xingjia, S. Hongxia, T.Q. Zheng. DTC in Doubly-fed VSCF wind turbine control system. *IEEE International Conference on Information Technologie (ICIT'06).* 15-17 December 2006. pp. 2715–2718.

[19] L.A. Serpa, J. W. Kolar, S. Ponnaluri, P. M. Barbosa. A Modified Direct Power Control Strategy Allowing the Connection of Three-Phase Inverter to the Grid through LCL Filters. *Industry Applications Conference, 40th IAS Annual Meeting (IAS'05),* Hong Kong, October 2005.

[20] D. Zhi, L. Xu. Direct Power Control of DFIG With Constant Switching Frequency and Improved Transient Performance. *IEEE Trans. On Energy Conversion*. Vol.22, No.1, March 2007. pp. 110-118.

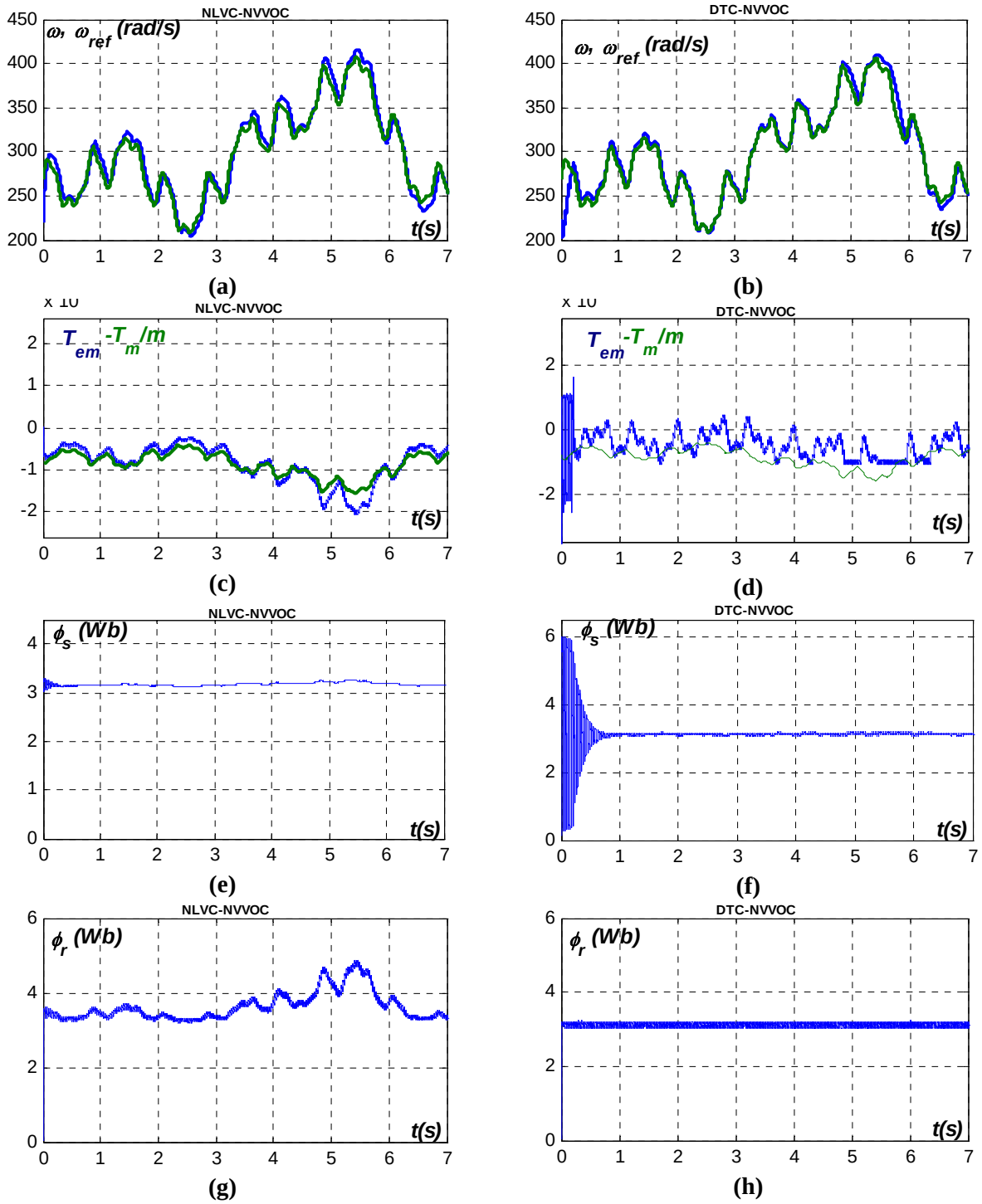

Fig.10 WECS Response under NLVC- NVVOC and DTC-NVVOC control strategies.
Legend: ω (a, b) , T_{em} (c, d) , φ_s (e, f) , φ_r (g, h)

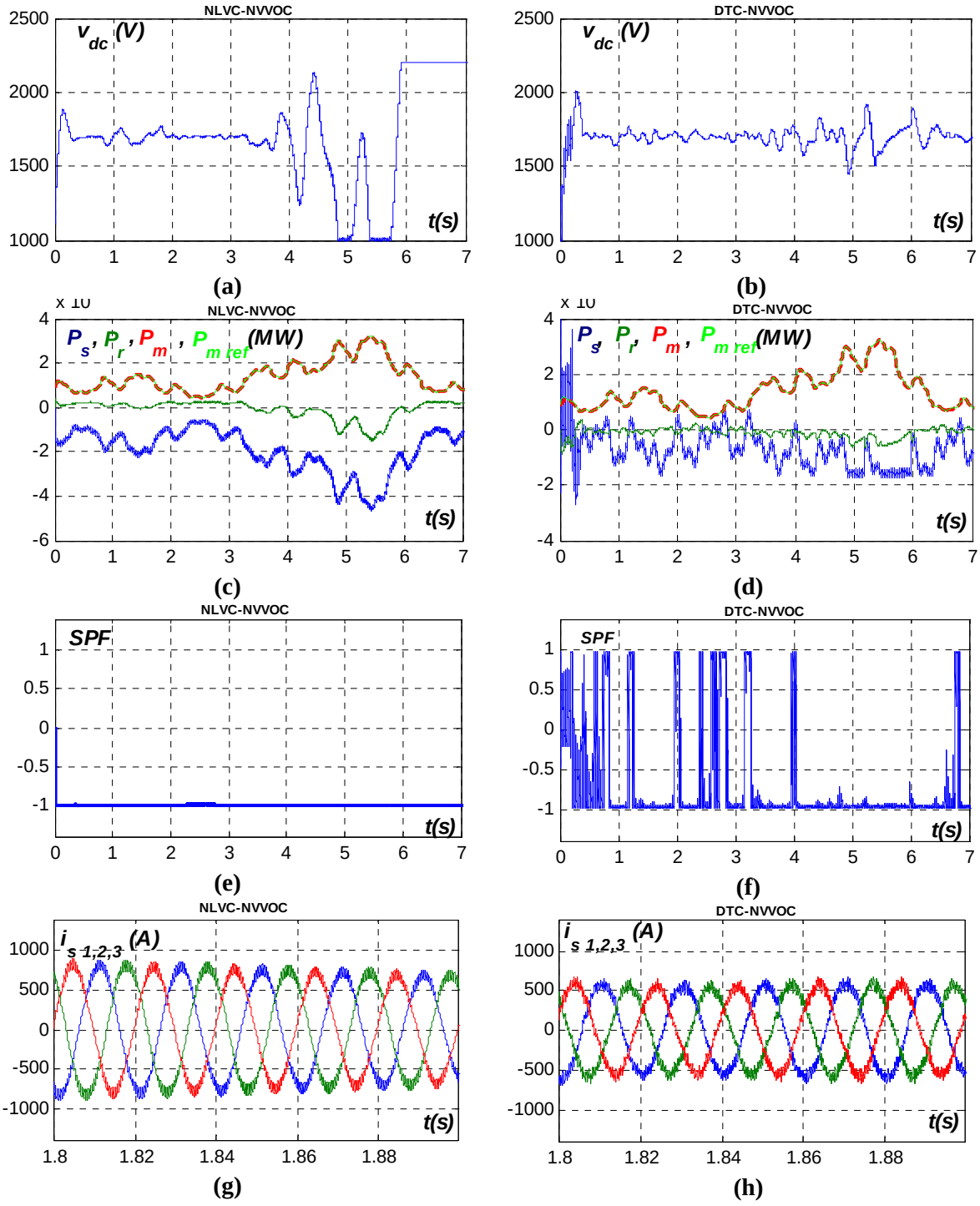

Fig.11 WECS Response under NLVC- NVVOC and DTC-NVVOC control strategies.
Legend: v_{dc} (a,b) ; P_s,P_r,P_m,P_{mref} (c,d) , SPF (e,f) , I_{s1}, I_{s2}, I_{s3} (g,h)

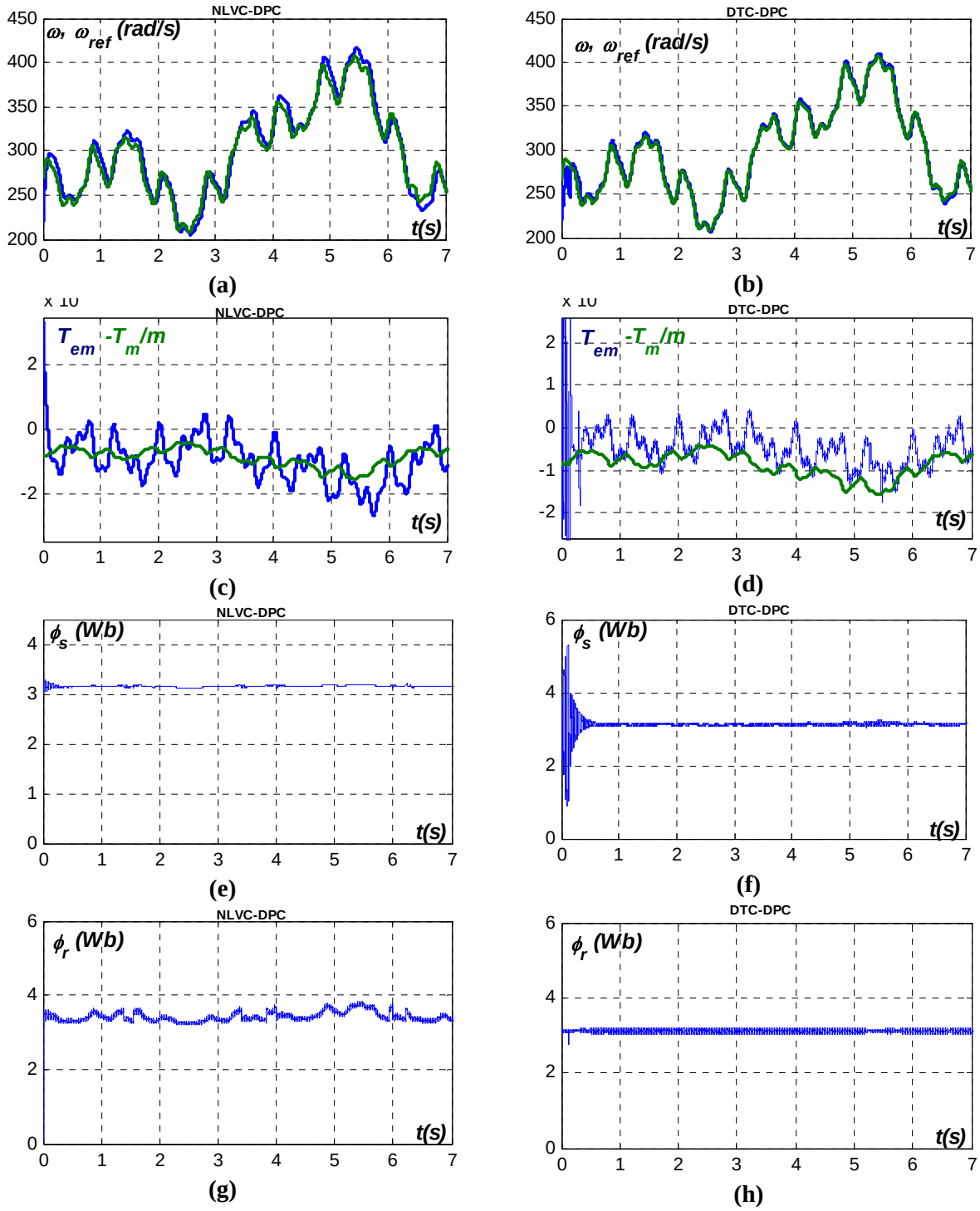

Fig.12 WECS Response under NLVC- DPC and DTC-DPC control strategies.
Legend: ω (a, b) ; T_{em} (c, d) ; φ_s (e, f) ; φ_r (g, h) ;

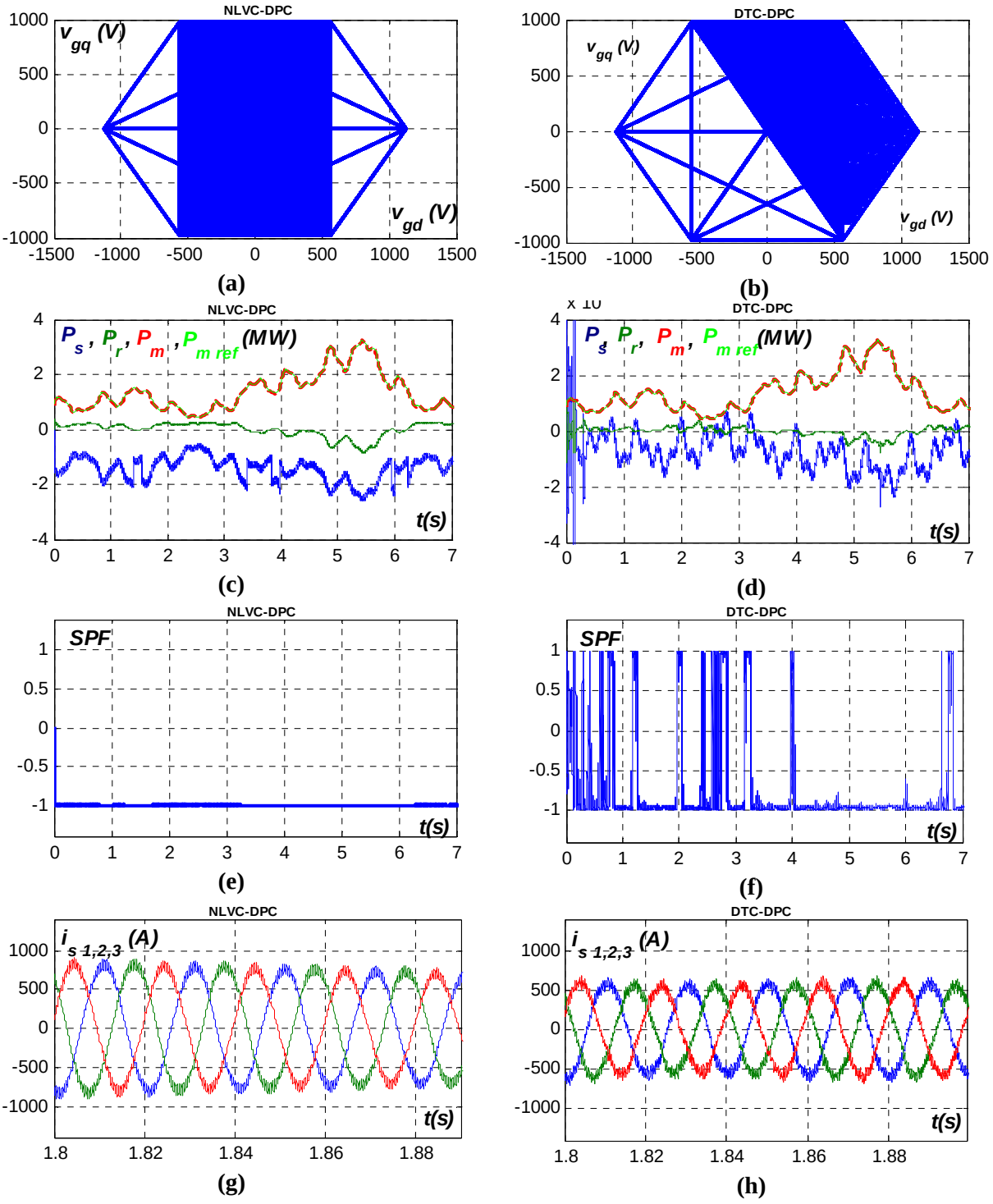

Fig.13 WECS Response under NLVC- DPC and DTC-DPC control strategies.
Legend: v_{gq} *vs.* v_{gd} (a,b) ; P_s,P_r,P_m,P_{mref} (c,d) ; *SPF* (e,f) ; I_{s1}, I_{s2}, I_{s3} (g,h)